



Estimation of some Radio Propagation Parameters using Measurements of Surface Meteorological Variables in Ede, Southwest Nigeria

A. A. Willoughby^a, M. E. Sanyaolu^a, M. O. Osinowo^a, A. O. Soge^a, O. F. Dairo^{b,*}

^aDepartment of Physical Sciences, Redeemer's University, P.M.B. 230, Ede, Osun State 232101, Nigeria

^bDepartment of Electrical and Electronic Engineering, Redeemer's University, P.M.B. 230, Ede, Osun State 232101, Nigeria

Abstract

A data acquisition system that utilised the open-source Arduino platform was developed to take real-time ground measurements of primary radio climatological variables of pressure, temperature, and relative humidity at Ede, a tropical station in southwest Nigeria (7.7349° N, 4.4439° E). Surface radio refractivity was deduced from these variables and used to estimate refractivity gradients at 100 m and 1000 m heights from the exponential reference atmosphere model for terrestrial propagation. Secondary radio propagation parameters such as refractivity gradients, the effective-earth-radius-factor, k , and geoclimatic factor, K , essential parameters for quick application in the planning and design of line-of-sight radio link systems, were also deduced. Data acquired from the device were compared to those obtained from the Re-Analyses (ERA-5) satellite database of the European Centre for Medium-Range Weather Forecast (ECMWF) 2020/2021. Aside from logging data on a micro secure digital (SD) card, measurements were displayed on a liquid crystal display (LCD). The peripheral Arduino-compatible meteorological sensors were connected to the analog inputs of the ATmega328 in the Arduino independent development environment (IDE), and the unit was powered by a 12 V battery charged by a 50-watt solar module. Results showed that slightly higher values of the ERA-5 data characterise the dry months from November to March, while the wet months displayed higher values of the Arduino-derived measured data. The accuracies of the data collected were compared using Mean Percentage Error (MPE) performance indicator. The interpretation is that the mean difference between the Arduino inferred measurements and the ERA-5 data is less than 10%, which is an indication of the measurement accuracy.

DOI:10.46481/jnsps.2023.875

Keywords: Arduino IDE, Refractivity gradients, Radio propagation, Multipath fading, Data acquisition

Article History :

Received: 19 June 2022

Received in revised form: 09 November 2022

Accepted for publication: 07 December 2022

Published: 11 December 2022

© 2022 The Author(s). Published by the Nigerian Society of Physical Sciences under the terms of the Creative Commons Attribution 4.0 International license (<https://creativecommons.org/licenses/by/4.0>). Further distribution of this work must maintain attribution to the author(s) and the published article's title, journal citation, and DOI.

Communicated by: M. Orosun

1. Introduction

Radio climatological research and system development rely on long-term data collected to monitor atmospheric parameters

or model data to design, develop, and implement various application systems. Some applications include meteorology and weather forecasting, climate change prediction, and terrestrial radio propagation models, which is the focus of this work. A fundamental parameter essential in studying the effects of the atmosphere on terrestrial radio propagation is the atmospheric refractive index, n , and its lapse rate, i.e., its gradient with al-

*Corresponding author tel. no: +234 8139567700
Email address: dairof@run.edu.ng (O. F. Dairo)

titude, dn/dh [1]. A scaled value of n is the refractivity, N , a useful input in radio propagation models. Radio climatological measuring instruments are expensive; hence it is possible to deduce the refractivity and associated radio parameters by taking surface measurements of pressure, temperature and relative humidity using the open-source Arduino Integrated Development Environment (IDE). Therefore, computing the surface refractivity, N_s , from data measured at the ground level enables the estimates of the radio propagation parameters to be deduced. This makes the data acquisition system (DAQ) developed using Arduino preferable to the expensive weather stations.

Measurements and data acquisition systems, in nearly all higher educational institutions in Nigeria that engage in data gathering for weather monitoring or other research purposes, are purchased from renowned manufacturers abroad [40, 41, 42]. The Nigerian Meteorological Agency (NIMET) and the Tropospheric Data Acquisition Network (TRODAN) are the major data repository agencies in the country, where almost all data analysts visit to obtain data for any region of interest in the country. Occasionally, a researcher may face difficulty obtaining data from these agencies because of the long-distance of the repository from the researcher's station or inconveniences and the cost of data purchase or requisition protocol. Some data retrieved are either missing with their dates skipped or unreliable, probably caused by natural or artificial noise interference. Also, the desired parameter may not even be in their inventory for logging.

Archiving credible and accurate data to meet international standards requires expensive and tested autonomous data loggers.

Against the backdrop of these constraints, the Department of Physical Sciences at Redeemer's University, Nigeria, designed a simple, affordable Arduino-based weather station for logging some common and valuable meteorological parameters in Ede, where the University is located. The following attributes were considered to achieve a functioning device: durability, affordability, and availability of hardware and software, easy construction and assembly of modules, standalone capability, high accuracy real-time data acquisition, conformance with international standards, easy data retrieval on an existing spreadsheet and easy adjustment of software code to allow for the addition of more sensors. It must also be quickly and easily replicated for interested research institutions. The Arduino IDE meets these criteria since it is more user-friendly and provides its hardware platform with a free download library and software coding or 'Sketch'. The data from the Arduino-based weather station were validated with ERA-5 satellite data, which provided data for meteorological variables at the ground surface, 100 m and 1 km above the ground. The European Centre for Medium-Range Weather Forecasts (ECMWF) Reanalysis fifth generation (v5) datasets popularly known as ERA-5 data, span a period of January 1950 to date. This work aims to develop an Arduino-based ground station to measure atmospheric pressure, temperature and relative humidity, which are the variables necessary to compute radio refractivity.

2. Background Theory

2.1. Radio Refractivity, N

Radio refractivity, N , and its gradient, dN/dh , are used by radio engineers for planning terrestrial radio links. Tropospheric refractivity gradients are created due to effects produced by individual components that constitute the atmospheric refractive index, i.e., pressure, temperature, and relative humidity [1, 2, 3, 4, 5, 6]. For example, due to the thermal heating of the atmosphere by the earth's surface in the upward direction, water vapour gradient and temperature differences between tropospheric layers resulting in convective air motion will give rise to negative temperature gradients. Radio refractivity is expressed in terms of these three meteorological variables:

$$N = (n - 1) \times 10^6 = \frac{77.6P}{T} + \frac{3.73 \times 10^5 e}{T^2} \quad (1)$$

where P is the atmospheric pressure in mb, the water vapour pressure, $e = e_s \times RH \times 0.01$ (mb), e_s being the saturation vapour pressure in mb, and RH is the relative humidity in %. e_s is obtained from $e_s = 6.11 \times 10^{a/(t+b)}$, where t is the temperature in °C, $a = 7.5$, $b = 237.3$ °C and T is the temperature in Kelvin [4-5, 7-9]. Equation (1) is valid for radio frequencies up to 100 GHz with less than 0.5% error [7-9]. The terms on the right-hand side of the equation represent the dry and wet terms of refractivity, respectively.

There are two methods of measuring n : the direct and indirect methods. The direct method employs a microwave refractometer, a somewhat costly instrument that is hardly in use in this part of the world. Although not as accurate or as expensive as the direct method, the indirect approach involves the measurements of weather observations of atmospheric pressure, temperature, and relative humidity, which are then converted to N in equation (1). Altitude profiles of N can also be obtained using the radiosonde. This telemetry instrument has attached a radio transmitter and sensors to it. It is launched into the atmosphere by a weather balloon. As it is climbing, it measures the three atmospheric variables, including wind speed and wind direction, transmitting the data at different altitudes by radio to a receiver at the ground station. Where a radiosonde is unavailable, height profiles of refractivity, N , can be estimated if monthly means of N_s are available by using the equation for the exponential reference atmosphere [6], which expresses the height dependence of refractivity:

$$N = N_s \exp\left(-\frac{h}{H}\right) \quad (2)$$

at altitude h , N_s is the refractivity at the ground level, and H is the scale height, the altitude at which refractivity has dropped to $1/e$ of surface refractivity and can either be derived empirically or from long term data in a particular region. For quick reference calculation of N at any height in equation (2), a global mean of $H = 7.35$ km [8] or tropical mean of 7.0 km may be adopted [10, 11].

2.2. Correlation between dN/dh and N_s and the effective earth radius factor, k

Investigations [2, 5, 6, 12] showed that a very good correlation is obtainable between the monthly averages of N_s and those of N gradients in the first kilometre above ground, which can be related as:

$$-\Delta N = A \exp(BN_s) \quad (3)$$

where $dN/dh \approx \Delta N$, ($dh = 1$ km), and A and B are constants derived for the region. From a ten-year database of daily radiosonde soundings, Willoughby et al. [5] deduced values of $A = 9.36$ and $B = 4.856E-03$ and a correlation of 0.78 for the whole of Nigeria, while Kolawole and Owonubi [12] obtained the values of $A = 2.30$ and $B = 8.630E-03$ and a correlation of 0.80 for the whole of Africa. $-\Delta N$ is used in estimating the effects of the atmosphere on the refraction of radio waves and the simplification of radio propagation engineering problems [5, 13, 14, 15, 16, 17]. Its variation produces the phenomena of scattering, scintillation and discontinuities or fading of propagated radio energy. It is also used in categorising if wave refraction is standard ($dN/dh = -40$ N/km), sub- ($dN/dh > -40$ N/km), super- ($dN/d < -40$ N/km), critical- ($dN/dh = -157$ N/km) refraction or ducting conditions ($dN/dh < -157$ N/km). These categories reveal atmospheric conditions that may be prevalent in a region, which may be inimical or conducive to the smooth propagation of radio waves. Thus, vertical dN/dh values are used to estimate path clearance and propagation associated effects such as ducting on trans-horizon paths [6, 7, 9]. In addition, surface reflection and multipath fading and distortion on terrestrial line-of-sight are occurrences caused by variations in dN/dh .

2.3. Effective Earth Radius Factor, k .

A model is usually adopted to calculate the effects of the atmosphere on radio waves. The model assumes that dN/dh is constant within the first kilometre above the ground. This concept permits radio rays to be drawn as straight rays over imaginary flat earth instead of curved rays over true earth of radius a . This results in an effective earth radius a_e and an effective earth radius factor, k , where $a_e = ka$. k has been given as [5, 6, 14, 18, 19]:

$$k = \left[1 + a \frac{dN}{dh} \times 10^{-6} \right]^{-1} \text{ or } \left[1 + a\Delta N \times 10^{-6} \right]^{-1} \quad (4)$$

Summarily, the statistics of N_s and the vertical gradient, dN/dh , are significant for the estimation of radio wave path clearance, multipath fading on terrestrial line-of-sight links and ducting effects on trans-horizon paths [7]. Also, the k value is used by radio engineers to calculate the distance to the radio horizon, d , of radio waves emanating from an antenna of height, h_{Tx} metres, i.e.,

$$d_{horizon} = \sqrt{2kah_{Tx}} \quad (5)$$

2.4. Geo-climatic factor, K

In a link design requiring the calculation of multipath fading and enhancement for path lengths greater than 5 km, a quick estimation of K for the average worst month for the geographic area of interest can be derived from [7, 19, 20, 21].

$$K = 10^{-4.6-0.0027dN_1} \quad (6)$$

where dN_1 is the point refractivity gradient in the lowest 65 m of the atmosphere not exceeded for 1% of an average year. For link design applications, the value of K from equation (6) is usually adopted to calculate the percentage of time that a fade depth A (dB) is exceeded from an average worst month. In this study, the lowest 100 m atmosphere has been considered. dN_1 values are usually obtained using interpolation techniques such as Inverse Distance Weighting (IDW) [20-21].

3. Methodology

By inserting values of A and B obtained from the models deduced [5, 12] for the tropical region in equation (3), estimates of $-\Delta N$ within the first km above ground can be made [15, 16, 17], thereby enabling the deduction of the k factor, geoclimatic factor and $d_{horizon}$, and other related radio propagation parameters. Refractivity-altitude profiles can also be obtained from equation (2). The computations will also determine if the models used in equations (2) and (3) can detect the various categories of refraction apart from normal refraction. In addition, multipath fading and enhancement modes can also be observed.

Numerous microcontroller-based data acquisition systems have been designed and developed to collect and process data on meteorological, agricultural, physical, and chemical processes [22 - 27]. In peripheral interface controllers (PIC)-based systems, the analog-to-digital (A/D) converter can be interfaced (for example, a PIC16F877) to record sensor signals and the data stored in a local erasable programmable read only memory (EPROM). This is unnecessary in the Arduino as both the A/D converter and EPROM are embedded in the IDE [28 - 39]. Adane et al. [22] built a meteorological DAQ using a PIC16F877A microcontroller to automatically retrieve instantaneous atmospheric pressure, temperature, and relative humidity measurements. The data were used to estimate, in real-time, the radio refractivity of air near the ground. This study exploited similar approach in estimating surface radio refractivity and related parameters in Ede from 2020 to 2021.

3.1. Circuit Design

3.1.1. Connections to the ATmega328

Figures 1 and 2 show the block diagram and circuit diagram of the setup and peripheral breakout shields to the Arduino analog and digital pins, respectively. The ATmega328 processor was used as a standalone without the Arduino board by connecting the bare minimum of components to make it function in Arduino IDE. The chip incorporates a six channel, 10-bit analog-to-digital converter (ADC) and a variety of communications ports including a serial peripheral interface (SPI). The following minimum external circuitry in Figure 1 is essential

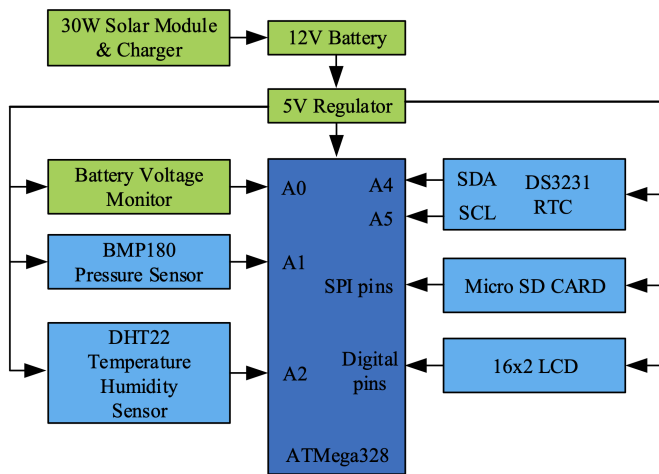


Figure 1. Sensor and breakout shield connection to Arduino input pins

to make the circuit function: a 16 MHz quartz crystal, X1, which determines the clock speed of the processor; two 22 pF capacitors, each connected from pins 9 and 10, respectively, to ground; a 12 V battery supplies power to a 7805 regulator, REG, which provides a positive 5 V to the whole circuit; the battery is charged by a solar panel; a 10 k Ω pull-up resistor, R1, from +5 V, (Vcc) to reset pin (1), prevents the chip from resetting itself during normal operation. The Arduino has six analog inputs, A0 to A5. Each input provides 10 bits of resolution (i.e., $2^{10} = 1024$). Thus the ADC can subdivide the analog signal into 1024 different values. By default, each analog signal input measures from ground to 5 V. For a 5 V reference and a 10-bit converter, the step size would be $5 \text{ V}/1024 = 4.88 \text{ mV}$. Analog sensors of pressure, temperature/relative humidity are each connected to the Arduino inputs, A1 and A2, respectively. LED (D2) indicates power on when the circuit is switched on. Filter capacitors C3 and C4 smooth out unwanted noise. The DS3231 real-time clock (RTC) pins, SDA and SCL are connected to the analog inputs A4 and A5 pins, respectively, of the ATmega328 as shown in Figure 1. Similarly, the Micro SD card is connected to the SPI pins on the microcontroller. A 16x2 LCD is connected to the appropriate digital pins on the ATmega328 microcontroller.

3.1.2. Atmospheric pressure sensing

The BMP180 breakout shield is a barometric pressure sensor with an I²C (“Wire”) interface. It

consists of a piezo-resistive sensor, an analog to digital converter and a control unit with E2PROM.

Very low noise - up to 0.02 hPa (17 cm) and fully calibrated Pressure Range of 300 hPa to 1100 hPa (+9000 m to -500 m) [43, 44]. It is ideally suited for barometric measurements. A power supply voltage of 1.8 V to 6 V is required to power the device. This sensor was connected to Arduino analog input, A1 [43, 44].

3.1.3. Temperature and relative humidity sensing

The AM2302 DHT22 Digital Temperature and Humidity Module is a temperature and humidity sensor with calibrated digital signal output. It uses dedicated digital module acquisition and temperature and humidity sensing technologies to ensure high reliability and excellent long-term stability. A capacitive sensing element and a high-precision temperature measurement element are used to sense relative humidity and temperature, respectively. The excellent quality of the device, its ultra-fast response, and cost-effective advantages makes it ideal for atmospheric measurements. Each sensor is calibrated in an extremely accurate humidity calibration chamber. Accuracy of measurement: 0-100%, ± 2 -5%. This sensor was connected to Arduino analog input, A2.

3.1.4. Battery voltage monitoring

A voltage divider comprising R2 (10k) and R3 (4k7) drops the voltage of a fully charged battery at 14 V to 4.48 V, that is, $[(4.7\text{k}/(10\text{k} + 4.7\text{k})) * 14 \text{ V}]$ to the microcontroller’s analog pin A0. This monitors the battery’s state, and the value is displayed on the LCD. 4.48 V is a reasonably safe input voltage for the analog input A0, since the Arduino analog inputs cannot accept voltages in excess of 5 V.

3.1.5. Date and Time keeping, RTC

The DS3231 AT24C32 I²C Precision Real-Time Clock (RTC) memory module for Arduino was used for date and time keeping. The device records and saves the year, month, day, hours, minutes, and seconds. The module incorporates a 3 V Lithium battery input and maintains accurate time keeping even when the main power supply is disengaged. Its SDA and SCL pins are connected to the analog input pins A4 and A5 of the Arduino, respectively as shown in the schematic of Fig. 2. The clock format can be programmed for 24 Hours or AM / PM 12-Hour format. The RTC library is available online from [47].

3.1.6. Data recording: Micro SD card reader module

A Micro Secure Digital (SD) storage expansion board Card Memory Shield compatible with the Arduino board was utilised for data storage. The interface between the ATmega328 and the SD card module is achieved by means of the high-speed SPI communication bus, capable of supporting simultaneous data transfer in master to slave directions and vice versa. On the Arduino Uno, the communication between the microcontroller and the SD card uses SPI, which takes place on digital pins 13, 11, and 12. Furthermore, SS pin 10 is used to select the SD card [48]. Data was logged at one-minute intervals.

3.1.7. Battery charging

Figure 4 shows a simple battery charging circuit. Schottky diode D1 prevents current flowback from the battery. U1, a three-terminal, adjustable precision shunt voltage regulator chip, is used to set a float charge voltage output of 13.8 V with the use of an external voltage divider, R4 and R5, i.e., $V_{\text{out}} = [1 + (10\text{k}/2\text{k}2)] \times 2.5$.

Once the reference voltage exceeds 2.5 V, the chip conducts and tries to maintain a constant output voltage determined by

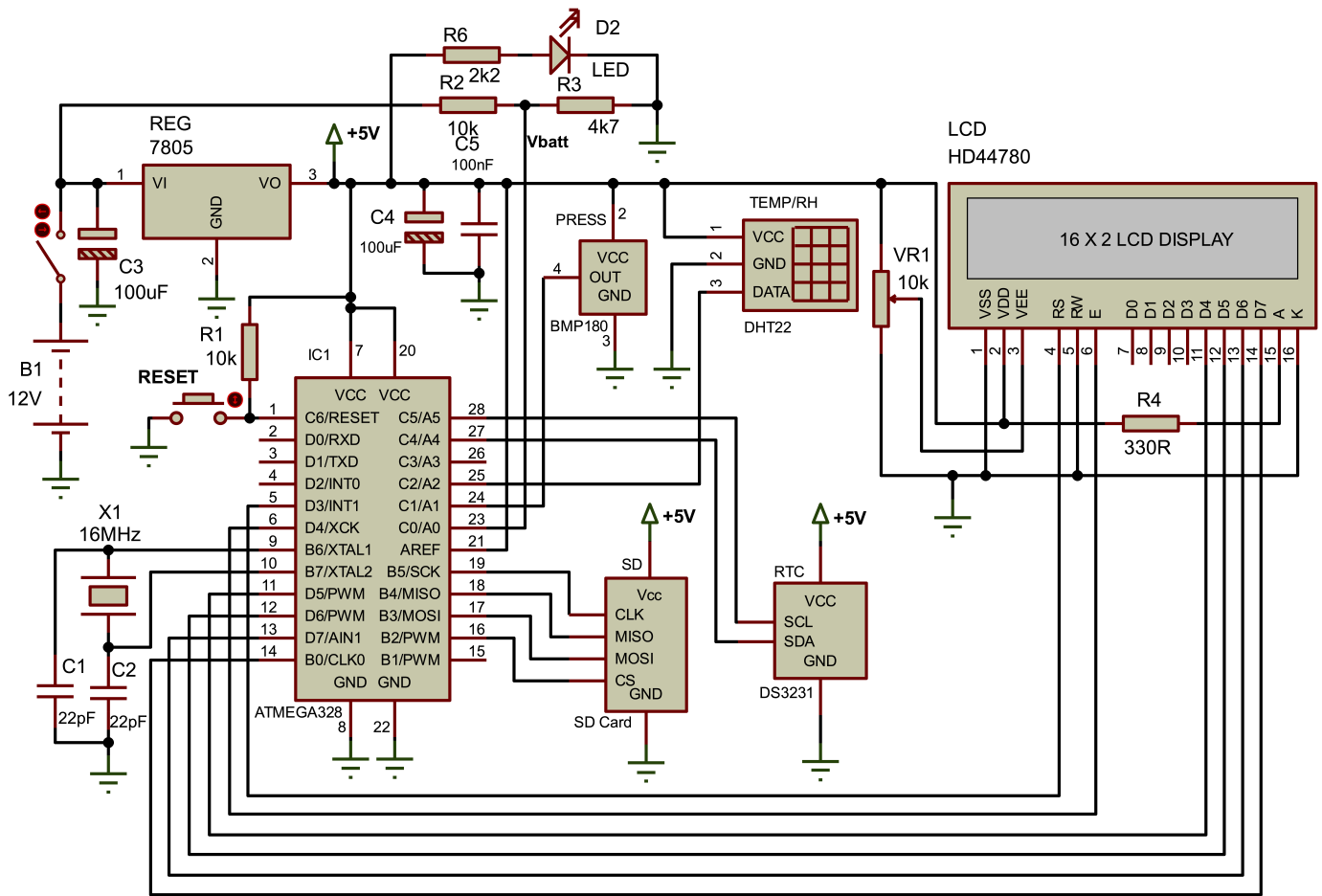
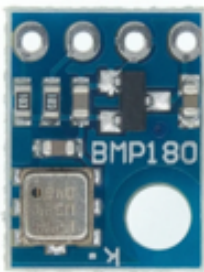


Figure 2. Schematic diagram of the Arduino set-up

Table 1. SPI implementation of SD card in the Arduino Uno

Designation	Function	Direction	Uno pin
SCLK	Serial clock	Output from Uno	13
MOSI	Master output/slave input	Output from Uno	11
MISO	Master input/slave output	Input to Uno	12
CS/SS	Chip select/slave select	Output from Uno	10
GND	Ground	Common	GND



(a)



(b)



(c)



(d)

Figure 3. Sensors: (a) BMP180 pressure sensor, (b) DHT22 temperature/humidity sensor, (c) DS3231 AT24C32 I2C Precision RTC Module, and (d) SD Card

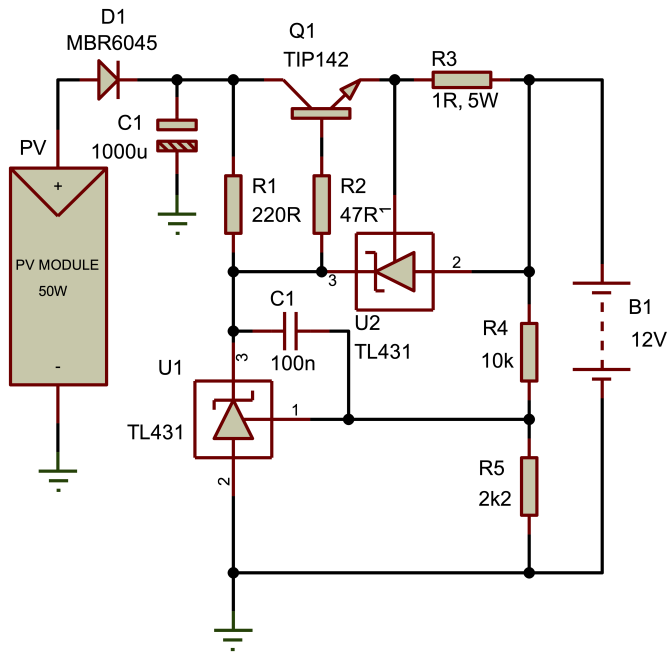


Figure 4. Simple battery charging circuitry from solar panel

the voltage divider of R1 and R2. U2, another adjustable Zener reference, in conjunction with R3, act as a current limiter from the TIP142 Darlington transistor Q1. If an over current occurs, the voltage developed across R3 causes the device to conduct, pulling down its pin 3, the cathode, towards the ground. This starves the base of Q1 of current, thus reducing the charging current. $I_{out} = V_{ref}/R3 = 2.5 \text{ V}/1 \Omega \approx 2.5 \text{ A}$. R3 is a 5 W resistor, since I^2R results in 2.5 W dissipation in the resistor.

3.2. Mean Absolute Percentage Error (MAPE)

The MAPE is commonly used in the evaluation of models as it is easily interpretable. A positive value of MAPE indicates over-estimation in the estimated values, while the negative value indicates under-estimation.

$$MAPE = \frac{\sum \left[\frac{|MEASUREMENT_i - ERA5_i|}{ERA5_i} \times 100 \right]}{n} \quad (7)$$

where $MEASUREMENT_i$ and $ERA5_i$ are the i th values of the measured and observed data, respectively. n is the number of data points.

4. Result and Discussion

The picture of the developed Arduino-based data acquisition system (DAQ) is shown in Figure 5.

Observations of Figures 6 to 13 show a general trend common to the monthly means of all the parameters. Mean values increase from January to April/May, fall to a minimum in August, rise to another peak in October/November, and decrease to lower values in December/January. Double peaks are thus exhibited annually. These values coincide with the two distinct seasonal patterns characteristic of the region. This southwest

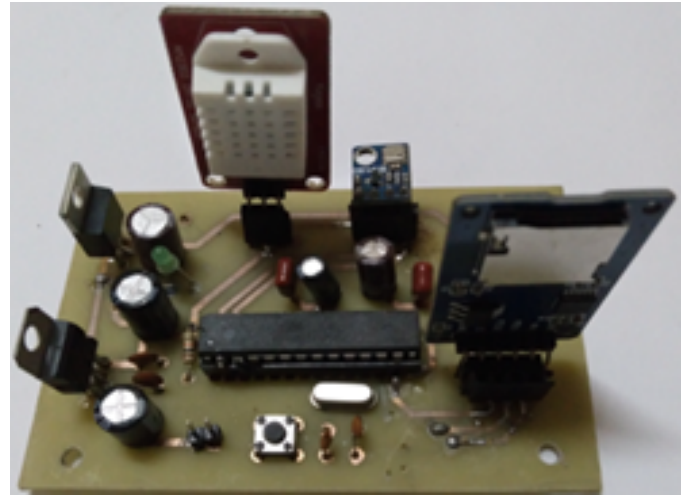


Figure 5. The PCB prototype of the Arduino DAQ (with ATmega328 processor in standalone mode)

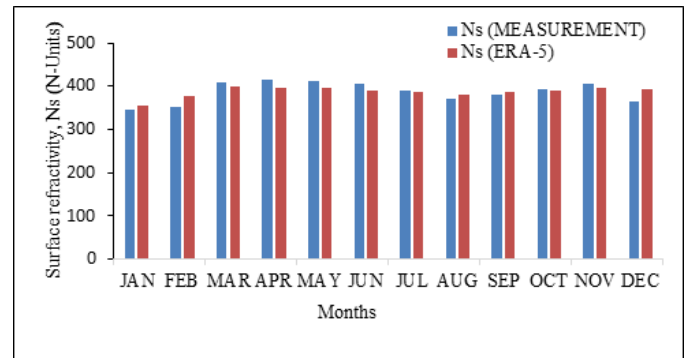


Figure 6. Comparison between ERA-5 and Arduino measurements of surface refractivity, Ns

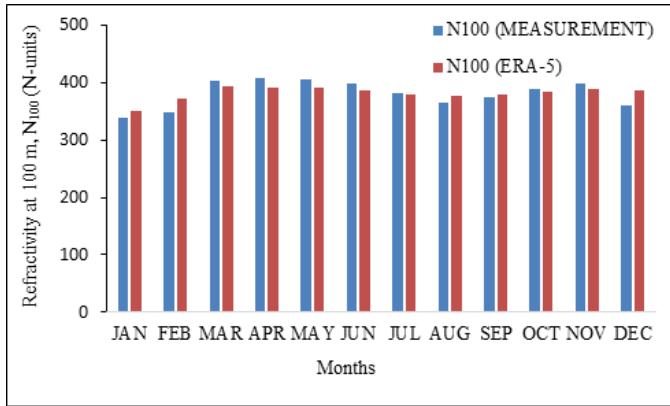
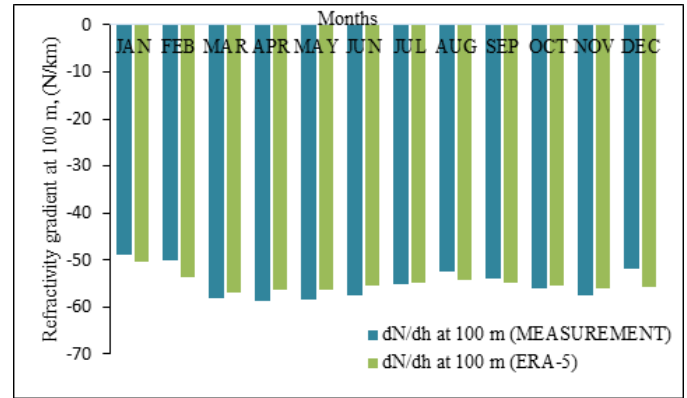
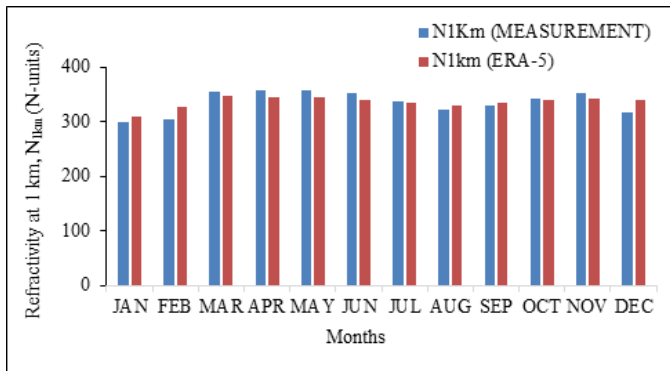
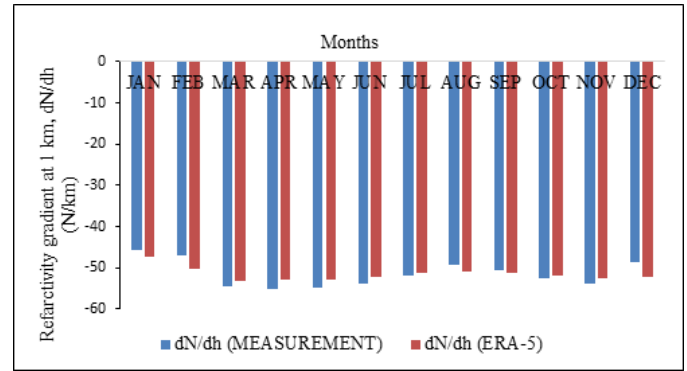
sub-region is annually under the influence of either the Harmattan or rainy seasons. Thus, the seasonal trends of the radio propagation parameters can be associated with the annual migration of the north-south movement Inter-Tropical Discontinuity (ITD), which effectively dictates the rainfall regime of the region [15]. The dip in August during the rainy season from May to October is coincidental with the brief cessation and subsequent reduction in rainfall in southwest Africa, despite the heavy incursion of the water vapour-laden maritime airmass emanating from the Gulf of Guinea. The dry season months from November to March exhibit lower values than the rainy season months from April/May to October [5, 11, 12, 13, 14, 18]. Generally, there is a slight trend in overestimating the ERA-5 data during the dry months, while the opposite is the case for the wet months when the Arduino measurements show slightly higher values.

Table 2 shows the comparisons of the results of the Arduino measurements to the corresponding monthly mean estimates from ERA-5 data.

Surface refractivity values obtained from the Arduino measurements are compared to those observed from the ERA-5 data and shown in Figure 5 below.

Table 2. Radio propagation parameters measured and compared with ERA-5 data

Parameters	Arduino Measurements	ERA-5 Data
1 Surface refractivity, N_s	$N(P_s, T_s, RH_s)$	Data
2 Refractivity (100 m), N_{100}	$N_s \exp(-0.1/7.0)$	Data
3 Refractivity (1 km), N_{1km}	$N_s \exp(-1.0/7.0)$	Data
4 Point Refractivity gradient (100 m), $-dN_1$	$(N_{100} - N_s)/(h_{100} - h_s)$	Data $(N_{100} - N_s)/(h_{100} - h_s)$
5 Refractivity gradient (1km), $-dN/dh$	$(N_{1km} - N_s)/(h_{1km} - h_s)$	Data $(N_{1km} - N_s)/(h_{1km} - h_s)$
6 Refractivity gradient (1km), $-dN$	$9.36 \exp(4.856E-03N_s)$	$9.36 \exp(4.856E-03N_s)$
7 Effective earth radius factor, k	$[1 + a \Delta N \times 10^{-6}]^{-1}$	Data $[1 + a dN/dh \times 10^{-6}]^{-1}$
8 Geoclimatic factor, K (100 m)	$10^{-4.6-0.0027*\Delta N_1}$	Data $10^{-4.6-0.0027*\Delta N_1}$

Figure 7. Comparison between ERA-5 and Arduino measurements of refractivity at 100 m, N_{100} Figure 9. Comparison between ERA-5 and Arduino measurements of point refractivity gradient at 100 m, dN_{100}/dh Figure 8. Comparison between ERA-5 and Arduino measurements of refractivity at 1 km, N_{1km} Figure 10. Comparison between ERA-5 and Arduino measurements of refractivity gradient at 1 km, dN_{1km}/dh

4.1. Performance Errors

The performance of the Arduino measured radio climatic parameters was tested against the ERA-5 data by computing the Mean Absolute Percentage Errors (MAPE) using Equation 7.

The MAPE measures the degree of error, high values indicate how far apart the measured and observed data are, therefore a high degree of error. The MAPE scores, shown in Table 3, give values less than 10%. The interpretation is that the mean difference between the Arduino and the ERA-5 data measurements is less than 10%, which is a very good measurement accuracy.

5. Conclusion

This study performed Arduino IDE measurements of ground-level primary radio climatological parameters of pressure, temperature, and relative humidity for 2020 and 2021. The study examined the expediency in using the measurements to estimate variables essential for designing radio propagation links within the lowest layers of the troposphere, which otherwise would have required radiosonde soundings. This scheme has facilitated the application of the exponential reference atmosphere in assessing refractivity gradient effects on radio signals. The measured data were compared with those obtained from the ECMWF ERA-5 satellite database. In general and from

Table 3. Performance errors (MAPE, %) for N_s and N_{1km}

Months	JAN	FEB	MAR	APR	MAY	JUN	JUL	AUG	SEP	OCT	NOV	DEC
MAPE (N_s)	6.16	8.60	3.35	0.11	1.26	0.94	0.42	1.78	3.77	3.55	0.16	1.31
MAPE (N_{1km})	2.25	0.92	8.14	4.93	5.71	3.29	5.19	0.04	2.26	0.46	7.57	9.47

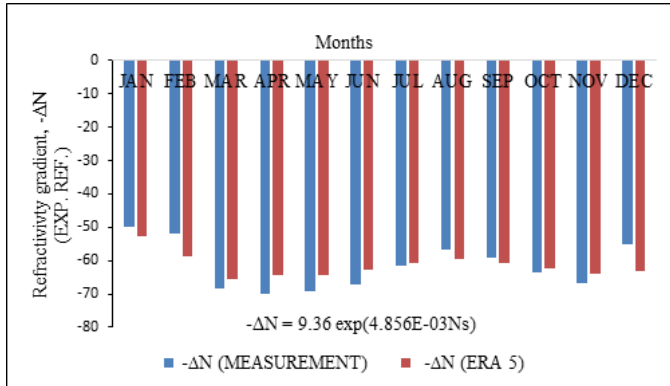


Figure 11. Comparison between ERA-5 and Arduino computations of exponential reference atmosphere

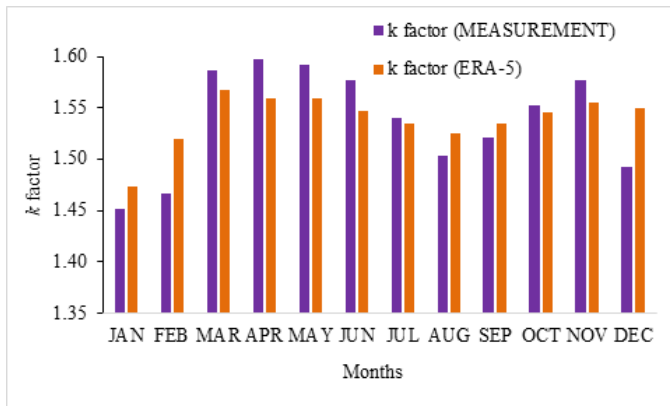
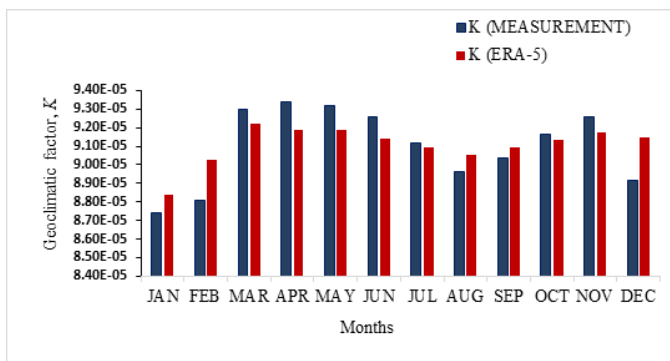
Figure 12. Comparison between ERA-5 and Arduino measurements of point refractivity gradient at 100 m, dN_{100}/dh 

Figure 13. Comparison between ERA-5 and Arduino measurements of Geoclimatic factor for 100 m height

previous works in the Nigerian southwest environment, radio climatic variables exhibit double peaks in April and November, with a minimum occurring in August. Dry months from

November to January are characterised by slightly higher values of the parameters obtained using the ERA-5 data compared to those obtained in the wet months. The Arduino measurements show marginally higher values than the ERA-5 data in the wet months, May to October, except August. The deviations seen in these values are not so appreciable to seriously affect procedures for calculating some refractive propagation effects on earth-satellite and terrestrial radio links. The less than 10% MAPE performance index suggests a high degree agreement between the Arduino device measurements and the ERA-5 data. Hence, this system is relatively accurate in implementing procedures for calculating refractivity effects on radio signals.

References

- [1] M. P. M. Hall, Effect of the troposphere on radio communication, IEEE Electromagnetic wave series, Peter Peregrinus Ltd, United Kingdom (1989) 105.
- [2] B. R. Bean, "The geographical height distribution of the gradient of refractive index", Proceedings of the IRE **41** (1953) 549.
- [3] J. A. Lane, "The radio refractive index gradient over the British Isles", Journal of Atmospheric and Solar-Terrestrial Physics, **21** (1961) 157.
- [4] E. K. Smith & S. Weintraub, "The constants in the equation for atmospheric refractive index at radio frequencies", Proc. IRE **41** (1953) 1035.
- [5] A. A. Willoughby, T. O. Aro & I. E. Owolabi, "Seasonal variations of radio refractivity gradients in Nigeria", Journal of Atmospheric and Solar-Terrestrial Physics **64** (2002) 417.
- [6] B. R. Bean & E. J. Dutton, Radio Meteorology, National Bureau of Standards Monograph **92** (1966) 9.
- [7] ITU-R P.530-16, Propagation data and prediction methods required for the design of terrestrial line-of-sight systems, International Telecommunication Union, ITU, Geneva, Switzerland (2015).
- [8] ITU-R Recommendation P.453-9, The radio refractive index: Its formula and refractivity data, International Telecommunication Union, ITU, Geneva, Switzerland (2003).
- [9] ITU-R Rec 834-4, Effects of Tropospheric Refraction on Radiowave Propagation, International Telecommunication Union, ITU, Geneva, Switzerland (2003).
- [10] A. T. Adediji, "Reduced-To-Sea-Level Value of Microwave Radio Refractivity Over Three Stations in Nigeria", Nigeria Journal of Pure and Applied Physics **7** (2017) 19.
- [11] L. B. Kolawole, "Climatological Variations of Surface Radio Refractivity in Nigeria", Bull. Nigeria Institute of Physics **4** (1980) 97.
- [12] L. B. Kolawole & J. J. Owonubi, "The surface radio refractivity over Africa", Nigerian Journal of Science **16** (1980) 441.
- [13] B. Adeyemi & I. Emmanuel, "Radio Refractivity Gradient over Nigeria using CM-SAF Satellite Retrieved Data", Nigerian Journal of Technological Research **7** (2012).
- [14] S. E. Falodun & P. N. Okeke, "Radiowave Propagation Measurements in Nigeria (Preliminary Reports)", Theoretical and Applied Climatology **113** (2013) 127.
- [15] O. F. Dairo & L. B. Kolawole, "Radio refractivity gradients in the lowest 100 m of the atmosphere over Lagos, Nigeria in the rainy-harmattan transition phase", Journal of Atmospheric and Solar-Terrestrial Physics **167** (2018) 169.
- [16] O. J. Abimbola, S. O. Bada, A. O. Falaiye, Y. M. Sukam, M. S. Otto & S. Muhammad, "Estimation of radio refractivity from satellite-derived meteorological data over a decade for West Africa", Scientific African **14** (2021) e01054, doi: 10.1016/j.sciaf.2021.e01054.

- [17] O. A. Falaiye, O. J. Abimbola, J. Omojola & D. S. Akinyanju, "Spacio-Temporal Variation of Radio Refractivity in Lafia, Nasarawa state using CM SAF ATOVS Satellite Data", *FULAFIA Journal of Science and Technology* **2** (2016) 111.
- [18] O. L. Ojo, J. S. Ojo & P. Akinyemi, "Characterisation of secondary radioclimatic variables for microwave and millimeter wave link design in Nigeria", *Indian Journal of Radio & Space Physics* **46** (2017) 83.
- [19] A. Abu-Almal & K. Al-Ansari, "Calculation of Effective Earth Radius and Point Refractivity Spatial Interpolation for Missing Data", *International Journal of Antennas and Propagation* **2010** (2010) 245070, doi: 10.1155/2010/245070.
- [20] I. J. Etokebe, M. C. Uko & I. U. Chiwe, "Determination of Refractivity Gradient and Geoclimatic Factor Using Radiosonde Data and Inverse Distance Weighting Spatial Interpolation for Missing Data", *International Journal of Systems Science and Applied Mathematics* **1** (2016) 76.
- [21] I. Emmanuel, B. Adeyemi & K. D. Adedayo, "Estimation of Refractivity Gradient and Geoclimatic Factor for Radio Link Design in Nigeria", *Physical Science International Journal* **19** (2018) 1, doi: 10.9734/PSIJ/2018/34489.
- [22] A. Adane, A. A. Yahia, E. Mameri & A. Adane, "Design of a Microcontroller-Based Data Acquisition System for Ground Weather Observations: Evaluation of Radio Refractivity of Air", *Int. J. Communications, Network and System Sciences* **7** (2014) 355.
- [23] M. Benghamen, "A low-cost wireless data acquisition system for weather station monitoring", *Renewable Energy* **35** (2010) 862.
- [24] M. Fuentes, M. Vivar, J. M. Burgos, J. Aguilera & J.A. Vacas, "Design of an accurate low-cost autonomous data logger for P.V. system monitoring using Arduino that complies with IEC standards", *Solar Energy Materials & Solar Cells* **130** (2014) 529.
- [25] S. Rosiek & F. J. Batlles, "A microcontroller-based data-acquisition system for meteorological station monitoring", *Energy Conversion Management* **49** (2008) 3746.
- [26] R. Mukaro & X. F. Carelse, "A microcontroller-based data acquisition system for solar radiation and environmental monitoring", *IEEE Trans. Instrumentation Measurements* **48** (1999) 1232.
- [27] R. Mukaro, X. F. Carelse & L. Olumekor, "First performance analysis of a silicon-cell microcontroller-based solar radiation monitoring", *Solar Energy* **63** (1998) 313.
- [28] K. E. Ukhurebor, I. C. Abiodun, S. O. Azi, I. Otete & L. E. Obogai, "A Cost-Effective Weather Monitoring Device", *Archives of Current Research International* **7** (2017) 1.
- [29] R. Sidqi, B. R. Rynaldo, S. H. Suroso & R. Firmansyah, "Arduino Based Weather Monitoring Telemetry System Using NRF24L01+", *IOP Conf. Series: Materials Science and Engineering* **336** (2018) 012024.
- [30] M. Ujoodha, A. Pultoo & A. Oojorah, "Climate Monitoring Using an Arduino-Based Mobile Weather Station and Open-Source Codes", *Journal of Education and Social Sciences* **16** (2020) 105.
- [31] D. Djuni & I. G. A. P. Raka Agung, "Design and Implementation of Arduino-Based Weather Monitoring System in Rural", *Journal of Electrical, Electronics and Informatics*, **3** (2020) 58, doi: 10.24843/JEEI.2019.v03.i02.p06.
- [32] S. N. Mahmood & F. F. Hasan, "Design of Weather Monitoring System Using Arduino Based Database Implementation", *Journal of Multidisciplinary Engineering Science and Technology (JMEST)* **4** (2017) 7109.
- [33] E. L. Omoze, T. J. Timiyo & P. E. Orukpe, "Development of an Automatic Weather Monitoring System", *IOSR Journal of Electrical and Electronics Engineering*, **14** (2019) 61.
- [34] J. Mabrouki, M. Azrou, D. Dhiba, Y. Farhaoui & S. El Hajjaji, "IoT-Based Data Logger for Weather Monitoring Using Arduino-Based Wireless Sensor Networks with Remote Graphical Application and Alerts", *Big Data Mining and Analytics* **4** (2021) 25, doi: 10.26599/BDMA.2020.9020018.
- [35] H. Saini, A. Thakur & N. Kumar, "Arduino based automatic wireless weather station with remote graphical application and alerts", *3rd International Conference on Signal Processing and Integrated Networks (SPIN)*. (2016) doi: 10.1109/SPIN.2016.7566768.
- [36] M. R. Laskar, R. Bhattacharjee, M. SauGiri & P. Bhattacharya, "Weather Forecasting using Arduino Based Cube-Sat", *Procedia Computer Science* **89** (2016) 320.
- [37] P. S. N. Reddy, D. V. Vardhan, K. T. K. Reddy & P. A. K. Reddy, "An IoT-based low-cost weather monitoring and alert system using node MCU", in *Smart Computing and Informatics*, S. C. Satapathy, V. Bhateja, and S. Das, eds. Singapore: Springer (2018) 265.
- [38] K. Krishnamurthi, S. Thapa, L. Kothari & A. Prakash, "Arduino Based Weather Monitoring System", *International Journal of Engineering Research and General Science* **3** (2015) 452.
- [39] V. Lakhara, P. Kurade, T. Pawar, A. Chougule & M. Asurlekar, "Real Time Weather Monitoring System Implementation Based on Internet of Things" Available at <http://dx.doi.org/10.2139/ssrn.3866819>.
- [40] O. L. Ojo, M. O. Ajewole, A. T. Adediji & J. S. Ojo, "Estimation of Clear-Air Fades Due to Radio Climatological Parameters for Microwave Link Applications in Akure, Nigeria", *International Journal of Engineering and Applied Sciences* **7** (2015) 1.
- [41] A. T. Adediji, "Reduced-to-Sea-Level Value of Microwave Radio Refractivity over three Stations in Nigeria", *Nigeria Journal of Pure and Applied Physics* **7** (2017) 19.
- [42] Centre for Atmospheric Research-National Space Research and Development Agency CAR-NASRDA. Available on-line: <https://carnasrda.com/trodan1/> (Accessed on 15th October 2021).
- [43] Spakfun.com. Available on-line: <https://learn.sparkfun.com/tutorials/bmp180-barometric-pressure-sensor-hookup/all>. (Accessed on 15th October 2021)
- [44] BMP180 Digital barometric pressure sensor. Available on-line: https://aebst.resource.bosch.com/media/_tech/media/product_flyer/BST-BMP180-FL000.pdf (Accessed on 15th October 2021)
- [45] Analog Devices. Available on-line: <https://www.instructables.com/How-to-use-DHT-22-sensor-Arduino-Tutorial/> (Accessed on 15th October 2021).
- [46] Project Hub. Available on-line: <https://create.arduino.cc/projecthub/mafzal/temperature-monitoring-with-dht22-arduino-15b013> (Accessed on 15th October 2021).
- [47] Adafruit. Available on-line: <https://learn.adafruit.com/adafruit-ds3231-precision-rtc-breakout/arduino-usage> (Accessed on 16th November 2021).
- [48] Arduino. Available on-line: <https://www.arduino.cc/en/Reference/SDCardNotes> (Accessed on 16th November 2021).